







Projected changes in the seasonal cycle of extreme rainfall events from CORDEX simulations over Central Africa

Thierry C. Fotso-Nguemo^{1,2}  · Ismaïla Diallo³  · Moussa Diakhaté⁴  ·
Derbetini A. Vondou^{2,5}  · Mamadou L. Mbaye⁶ · Andreas Haensler⁷ ·
Amadou T. Gaye⁴ · Clément Tchawoua⁸

Received: 20 March 2018 / Accepted: 4 July 2019 / Published online: 18 July 2019
© Springer Nature B.V. 2019

Abstract

This study explores the potential response of the seasonal cycle of extreme rainfall indices over Central Africa (CA) to the global warming for both the middle (2029–2058) and late twenty-first century (2069–2098), based on analysis of multi-model ensembles mean of fifteen regional climate models (RCMs) simulations. Although few dry/wet biases are still evident, for the present day climate, the RCMs ensemble mostly outperforms the driving global climate models, with a better representation of the seasonal cycle of various rainfall indices over two key sub-regions of CA chosen according to their particular rainfall patterns. Both middle and late twenty-first century project a non-significant decrease in total wet-day rainfall amount over the two analysed sub-regions, with peaks found during pre-monsoon months. We also found a significant decrease in wet-day frequency which was consistent with decreases in total wet-day rainfall amount, while wet-day intensity is projected to significantly increase. These results suggest that the decrease in total wet-day rainfall amount could be associated with less frequent events and not with their intensity. The results also have shown that dry (wet) spells are projected to significantly increase (decrease) over both sub-regions with shorter (longer) dry (wet) spells projected during pre-monsoon months. Consequently, countries within these two sub-regions could experience a more extended dry season, and therefore would be exposed to high drought risk in the future under global warming. However, changes in maximum 1-day rainfall amount, maximum 5-day rainfall amount, and 95th percentile are projected to significantly increase during monsoon months, with the maximum 1-day rainfall amount recording largest increases. Additionally, the total amount of rainfall events above the 95th percentile projects a significant increase of about 10–45 % during monsoon months, while the total number of occurrence of rainfall events above the 95th percentile projects a slight significant decrease of 4–8 % during pre-monsoon

Electronic supplementary material The online version of this article (<https://doi.org/10.1007/s10584-019-02492-9>) contains supplementary material, which is available to authorized users.

✉ Thierry C. Fotso-Nguemo
fotso.nguemo@gmail.com

Extended author information available on the last page of the article.

months but more pronounced for the late twenty-first century. This implies that in the future, extremes rainfall events could be more intense both in terms of rainfall amount and intensity during monsoon months. Such changes are likely to amplify the probability of flood risks during monsoon months over CA, particularly the two sub-regions. This study could therefore be an important input for disaster preparedness, adaptation planning, and mitigation strategies for Central African countries.

1 Introduction

Climate variations and change are induced by internal and external factors, which include natural external forcings (e.g., solar radiation and volcanism) and anthropogenic forcings (e.g., greenhouse gas (GHG) emission, aerosol and land use, and land cover changes). Change in extreme weather conditions is generally the result of external forcings that affect various aspects of the climate system (Seneviratne et al. 2012). The rapid increase of GHG concentration, which is considered as main driver of change in extreme events, is a real threat for Central African countries. Populations of this region of Africa are particularly vulnerable to extreme events not only because of their low adaptive capacity, but also of the fact that their economy is mainly based on agriculture, breeding, and hydroelectric power generation (Sonwa et al. 2012). However, extreme weather events, such as floods and severe drought, can directly or indirectly impact many socio-economical sectors, such as rain-feed agriculture, infrastructures, water resources availability, hydroelectric power generation, populations displacement, social riots, and loss of human lives (Saha 2015; Tanessong et al. 2017; Almer et al. 2017). To tackle these potential obstacles to the socio-economic development of countries of this region, it becomes urgent to conduct investigations leading to better understand the causes of the observed changes, which will help policy and decision-makers to develop mitigation and adaptation strategies in accordance with the twenty-first Conference Of Parties (COP21) held in Paris (Jacquet and Jamieson 2016).

It is well known that rainfall is one of the most important climatic variables. Its increasing use to study the patterns as well as projections of climate extremes in Africa has demonstrated this importance (e.g., Haensler et al. 2013; Diallo et al. 2014; Dosio et al. 2015; Sylla et al. 2015; Pinto et al. 2016; Klutse et al. 2016; Vondou and Haensler 2017; Fotso-Nguemo et al. 2018; Pokam et al. 2018; Sonkoué et al. 2018; Tamoffo et al. 2019, among others). In this context, based on an multi-model ensemble mean of a combined set of regional climate models (RCMs) and global climate models (GCMs), both completed respectively in the framework of the COordinated Regional climate Downscaling EXperiment (CORDEX; <http://www.cordex.org>; Giorgi et al. 2009) and the phase 5 of the Coupled Model Intercomparison Project (CMIP5; <https://cmip.llnl.gov/cmip5/>; Taylor et al. 2012), Haensler et al. (2013) investigated changes in the intensity of heavy rainfall events over Central Africa (CA). Their results show that intensity of heavy rainfall events will significantly increase for both high and low GHG emission scenarios. The results of other authors are consistent with that of Haensler et al. (2013), also showing increasing trend in heavy rainfall events across CA (Fotso-Nguemo et al. 2018; Pokam et al. 2018; Sonkoué et al. 2018). Such change was linked to the increase of moisture convergence for which the Congo Basin rainforest plays an important role (Dyer et al. 2017). On the other hand, the investigations carried out over other regions of Africa also suggest a general increase in extreme rainfall event, mostly driven by an intensification of the hydrological cycle (Sylla et al. 2015; Diallo et al. 2016; Pinto et al. 2016). Through these works, it appears that rainfall change induced by enhanced

anthropogenic GHG concentrations is expected to become more frequent and more intense over some parts of Africa at the end of the twenty-first century. In addition, according to the Fifth Assessment Report of the Intergovernmental Panel on Climate Change (IPCC), the frequency of heavy rainfall events and severe droughts will increase worldwide, particularly over tropical and sub-tropical regions (IPCC 2013).

It is now established that anthropogenic climate change will have as consequence a change in rainfall patterns over Africa, which could result in more extensive dry seasons and shorter rainy seasons (Diallo et al. 2012; Mariotti et al. 2014; Sylla et al. 2015; Fotso-Nguemo et al. 2017). However, in comparison with other regions of Africa, CA has not received so much attention for understanding of either climate drivers (Vondou et al. 2010; Pokam et al. 2014; Kamsu-Tamo et al. 2014; Cook and Vizzy 2015; Hua et al. 2016; Zebaze et al. 2017; Dyer et al. 2017; Dommo et al. 2018) or extreme weather events (Haensler et al. 2013; Vondou and Haensler 2017; Fotso-Nguemo et al. 2018; Pokam et al. 2018; Sonkoué et al. 2018; Tamoffo et al. 2019). Despite the fact that assessment of changes in extreme weather events has been performed from multi-model ensemble mean of several models, the analyses of these authors were more focused on the spatial distribution of these events. In addition, to our knowledge, no studies have yet been conducted to investigate how these events and their intensities will change throughout the seasonal cycle of the Central African monsoon (CAM). However, such changes could probably affect the occurrence of extreme rainfall events at seasonal time scale. Additionally, the timing of these changes and the way in which the length of the seasons is changed can worsen the resulting impacts. It would therefore be interesting to evaluate the seasonal cycle pattern of changes in the extreme rainfall indices, related to changes in the CAM.

This study utilizes a multi-model ensemble mean of RCM simulations which consists of a total of fifteen (15) RCM members, to firstly explore the response to increasing GHG concentrations on the projected seasonal cycle of ten extreme rainfall indices for the middle and late twenty-first century over CA. Understanding and estimating the changes in the seasonal cycle of these extreme rainfall events could be an important input for the disaster preparedness, adaptation planning, and mitigation strategies for the region's countries. In the next section, we give a brief description of dataset as well as the methodology used in this study. In Section 3, results for current climate and also for climate change projections obtained through the analysis of extreme rainfall indices applied to daily rainfall time series are presented. Summary of the findings and main conclusions are presented in Section 4.

2 Datasets and methodology

In this work, six RCMs from CORDEX-Africa experiments are used to dynamically downscale seven GCMs from CMIP5. The summary of the fifteen considered RCM members, resulting from the dynamical downscaling of different GCMs, is displayed in Table 1. All downscaling experiments were performed at 50 km horizontal grid spacing resolution ($\sim 0.44^\circ$), over the same numerical domain covering the African continent, over a period of 150 years distributed as follows: historical simulations, forced by a combination of natural and anthropogenic atmospheric conditions, cover the period from 1950 to 2005; while the future simulations, which are forced by the high GHG-forcing namely representative concentration pathways scenario (RCP8.5; Moss et al. 2010), cover the period from 2006 to 2100. A detailed description of the CORDEX and CMIP5 experimental set-ups can be found in Nikulin et al. (2012) and Taylor et al. (2012) respectively. Note, for each RCMs and GCMs

Table 1 List of RCMs and driving GCMs

Institute	RCMs	Driving GCMs	Spatial resolution	Source
CLM-Com	CCLM	CNRM-CM5 EC-EARTH MPI-ESM-LR HadGM2-ES	0.44° × 0.44°	Germany
DMI	HIRHAM	EC-EARTH	0.44° × 0.44°	Denmark
CNRM	ALADIN	CNRM-CM5	0.44° × 0.44°	France
KNMI	RACMO	EC-EARTH HadGM2-ES	0.44° × 0.44°	Finland
SMHI	RCA4	EC-EARTH MIROC5 MPI-ESM-LR NorESM1-M	0.44° × 0.44°	Sweden
GERICS	REMO	EC-EARTH IPSL-CM5A-LR MPI-ESM-LR	0.44° × 0.44°	Germany

For a full description of the models' setup see, Nikulin et al. (2012) and Taylor et al. (2012) for RCMs and GCMs, respectively

output members, three 30-year time slice periods of daily rainfall were chosen over the Central African domain shown in Fig. 1 as follows: one historical (1976–2005) representing the recent past and, two futures (2029–2058) and (2069–2098) referring respectively to the middle and the late twenty-first century.

We considered ten climate indices defined by the Expert Team on Climate Change Detection and Indices (ETCCDI; Zhang et al. 2011), in order to measure daily rainfall characteristic and extreme events (see, Table 2 for details). These indices, which are increasingly used by researchers around the world, have shown their effectiveness in detecting, attributing, and predicting changes in extreme weather conditions over several regions of Africa (e.g., Sylla et al. 2015; Pinto et al. 2016; Diallo et al. 2016; Pokam et al. 2018; Sonkoué et al. 2018). To obtain the time series of the data used to represent the seasonal cycle of these indices, we proceeded as follows: firstly, each index is computed on every land grid point for each month of the daily time series and then the long-term average for each month of the year is calculated over the simulated 30 years. The multi-model ensemble mean for each month including the contribution of each experiment is then constructed for the historical and the projections.

To evaluate the performance of both GCMs and RCMs ensemble mean models in simulating daily rainfall indices over CA during the historical period, we compare their results with those of the ensemble mean of seven gridded observation products (Obs thereafter) over a common time period across models and Obs (1998–2005). Note that, indices were calculated using each Obs dataset, and the ensemble average of those results were used. These Obs, which are archived and freely accessible, were built spatially and temporally by interpolating ground-based and satellite data records. It should be mentioned that, despite

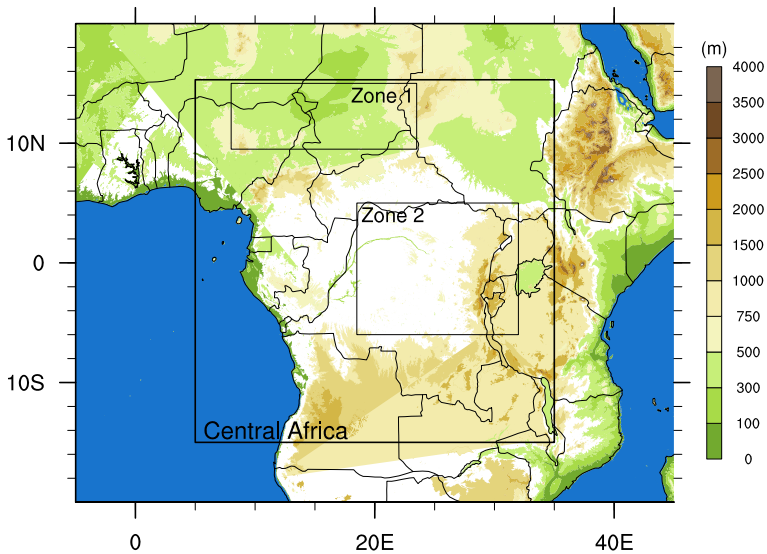


Fig. 1 Central Africa topography and selected sub-regions for analysis

the fact that these Obs may have some uncertainties due to either ground-based measurement or satellite measurement bias, they have recently shown a remarkable performance over Africa where daily rain gauge datasets are rare and very scarce if they exist (Nikulin et al. 2012; Sylla et al. 2013). More information on the characteristics of the different Obs used are summarized in Table 3. For consistency purpose between RCMs, GCMs, and Obs during the historical period, the datasets are interpolated onto the RCMs' grid spacing (0.44°) as follow: all data with finer resolution than 0.44° are remapped using a distance-weighted interpolation method, while all other data, with coarser resolution than 0.44° , are interpolated through the bilinear interpolation method.

The agreement between simulated and observed daily rainfall indices during the historical period is further evaluated using the Taylor diagram (Taylor 2001), which quantifies the similarity between simulations and Obs in terms of correlation (PCC; pattern correlations coefficient), centred root mean square error (RMSE), and amplitude of variability (SD; standard deviation). In order to measure the model agreement and thus the reduction of uncertainty in the projected changes, the climate change signal of the RCM ensemble mean is considered as significant if more than 80 % of RCMs used (i.e., more than 12 out of 15 members) agree on its sign.

All analysis on the seasonal cycles of daily rainfall indices will be done over two key sub-regions (zone 1 and zone 2) identified in Fig. 1. These sub-regions are characterized by a different behavior of the rainy season (see Fotso-Nguemo et al. 2016 for more details on the main characteristics of the climate regime of the two sub-regions used). Note, the analysis on the spatial distributions of daily rainfall indices will be made for all seasons of the Central African domain, i.e., December–January–February (DJF), March–April–May (MAM), June–July–August (JJA), and September–October–November (SON).

Table 2 Definitions of the indices of rainfall extremes

Label	Index name	Index definition	Units
PRCPTOT	Total wet-days rainfall amount	Total rainfall from wet-day. Let $RR_{i,j}$ be the daily rainfall amount on day i in period j . If I represent the number of day in i , then $PRCPTOT_j = \sum_{i=1}^I RR_{i,j}$	mm
RR1	Total wet-day rainfall	Number of days with rainfall amount ≥ 1 mm. Let $RR_{i,j}$ be the daily rainfall amount on day i in the period j . Count the number of day were $RR_{i,j} \geq 1$ mm	day
SDII	Simple daily intensity indices	Average rainfall from wet-days. Let $RR_{w,j}$ be the daily rainfall amount on wet-day, $RR \geq 1$ mm in period j . If W represents number of wet-day in j , then: $SDII_j = (\sum_{w=1}^W RR_{w,j})/W$	mm/day
CDD	Consecutive dry days	Maximum number of consecutive dry days. Let $RR_{i,j}$ be the daily rainfall amount on day i in the period j . Count the largest number of consecutive day were $RR_{i,j} < 1$ mm	day
CWD	Consecutive wet-days	Maximum number of consecutive wet-days. Let $RR_{i,j}$ be the daily rainfall amount on day i in the period j . Count the largest number of consecutive day were $RR_{i,j} \geq 1$ mm	day
RX1DAY	Highest 1-day rainfall amount	Maximum daily rainfall amount. Let $RR_{k,j}$ be the daily rainfall amount on day k in the period j . The maximum daily values for the period j are: $RX1DAY_j = \max(RR_{k,j})$	mm
RX5DAY	Highest 5-day rainfall amount	Maximum rainfall sum for 5-day interval. Let $RR_{k,j}$ be the rainfall amount for the 5-day interval ending k in period j . The maximum 5-day values for the period j are: $RX5DAY_j = \max(RR_{k,j})$	mm
R95	95th percentile	The 95th percentile of daily rainfall events is the value above which 5 % of the daily rainfall events are found	mm/day
R95P	Total wet-day frequency above the 95th percentile	Number of days with rainfall amount ≥ 95 th percentile. Let $RR_{i,j}$ be the daily rainfall amount on day i in the period j and let RR_{w95} be the 95th percentile of rainfall on wet-day in the baseline period (1986–2005). Count the number of day were $RR_{i,j} \geq RR_{w95}$	day
R95PTOT	Total wet-days amount above the 95th percentile	Total rainfall from days with $RR \geq 95$ th percentile of the distribution of daily rainfall amount at day with 1 mm or more rainfall in the 1986–2005 baseline period. Let $RR_{w,j}$ be the daily rainfall amount on a wet-day w ($RR \geq 1$ mm) in period i and let RR_{w95} be the 95th percentile of rainfall on wet-day in the baseline period (1986–2005). If W represent the number of wet-day in the period, then: $R95P_j = \sum_{w=1}^W RR_{w,j}$, where $RR_{w,j} \geq RR_{w95}$	mm

For a complete list and definitions of ETCCDI indices see, Zhang et al. (2011)

Table 3 Description of daily observation datasets

Product name	Definition	Spatial resolution	Reference
ARC	African Rainfall Climatology, version 2	$0.1^\circ \times 0.1^\circ$ 1983 – present	Novella and Thiaw (2013)
CHIRPS	Climate Hazards group InfraRed Precipitation with Stations, version 2.0	$0.25^\circ \times 0.25^\circ$ 1981 – present	Funk et al. (2014)
CMORPH	Climate Prediction Center morphing method	$0.25^\circ \times 0.25^\circ$ 1998 – present	Joyce et al. (2004)
GPCP	Global Precipitation Climatology Project, version 2.1	$1.0^\circ \times 1.0^\circ$ 1996 – present	Huffman et al. (2009)
MSWEP	Multi-Source Weighted-Ensemble Precipitation, version 1.1	$0.25^\circ \times 0.25^\circ$ 1979 – present	Beck et al. (2017)
PERSIANN	Precipitation Estimation from Remotely Sensed Information using Artificial Neural Networks, vresion 1	$0.25^\circ \times 0.25^\circ$ 1983 – present	Ashouri et al. (2015)
TRMM	Tropical Rainfall Measuring Mission, 3B42	$0.25^\circ \times 0.25^\circ$ 1998 – 2015	Huffman et al. (2007)

3 Results and discussion

3.1 Evaluation of extreme rainfall indices

3.1.1 Duration and intensity-based indices

Figure 2 presents the mean seasonal cycle of total wet-day rainfall amount (PRCPTOT; first row), wet-day frequency (RR1; second row), wet-day intensity (SDII; third row), dry spell (CDD; fourth row), and wet spell (CWD; fifth row), from Obs ensemble mean (black), GCM ensemble mean (red), and RCMs ensemble mean (blue), averaged over zone 1 (first column) and zone 2 (second column), during the historical period (1998–2005). Over zone 1, the seasonal cycle of PRCPTOT from Obs shows a single-peaked rainy season. This rainy season starts in March–April, peaks in August at the northernmost extent of the Inter-Tropical Convergence Zone (ITCZ), and retreats in October–November. Conversely to zone 1, over zone 2, the seasonal cycle of PRCPTOT shows a double-peaked rainy season associated with the latitudinal migration of the ITCZ. The first maximum occurs in April when the ITCZ moves northward, while the second takes place in November when the ITCZ retreats to the south. Comparing Obs with RCMs and GCMs, it is evident that the main features of the seasonal timing of PRCPTOT are reasonably captured, though some discrepancies between models and Obs can be noticed. For instance, GCMs produce larger PRCPTOT over zone 2, which is more accentuated during the rainy seasons (bias of up to 50 mm). It is worth mentioning that similar feature is also noted during March–June over zone 1, where both RCMs and

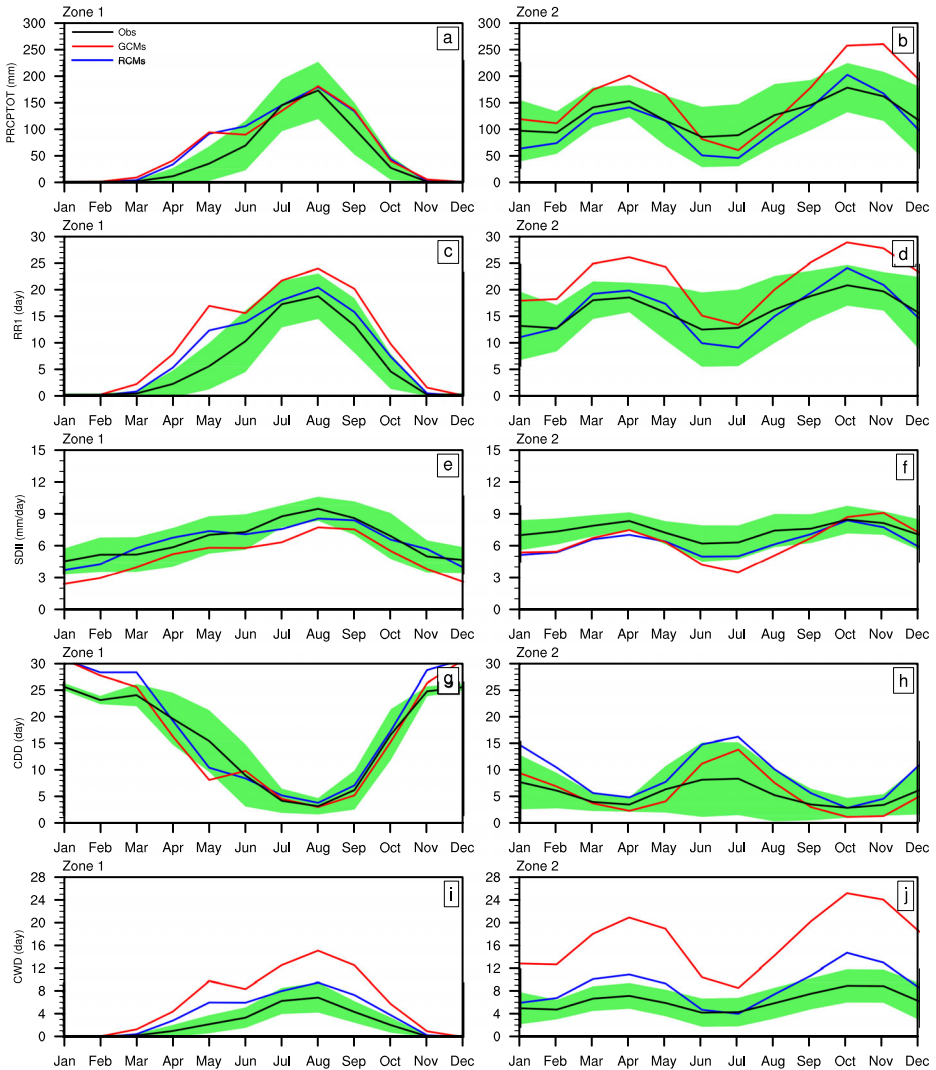


Fig. 2 Mean (1998–2005) seasonal cycles for total wet-day rainfall amount (PRCPTOT; **a, b**), wet-day frequency (RR1; **c, d**), wet-day intensity (SDII; **e, f**), dry spell (CDD; **g, h**) and wet spell (CWD; **i, j**), over zone 1 (first column) and zone 2 (second column), from Observations ensemble mean (black), GCM ensemble mean, and RCM ensemble mean (blue). Green shading corresponds to the full range of observations datasets

GCMs overestimate PRCPTOT. This is also reflected by the fact that RCMs have a better variability than GCMs compared with Obs, despite their smaller PCC which still remains >0.6 (see supplementary material; Fig. S1; sky blue).

The seasonal cycle of RR1 and SDII clearly shows that Obs and models provide a substantially different description of daily rainfall. Furthermore, the double-peak structure found in PRCPTOT over zone 2 is evident for RR1 and SDII. Contrary to the results found over the West African Guinean region (Sylla et al. 2015; Diallo et al. 2016), our

results reveal that in addition to wet-day frequency, wet-day intensity also contributes to the bimodal structure of the seasonal cycle of rainfall in zone 2. The RR1 curves clearly show that RCM simulations improve that of GCMs in both sub-regions, by producing number of wet-day occurrences closer to that of Obs despite some discrepancies (also see supplementary material; Fig. S1; yellow). Particularly for the SDII, the range of Obs uncertainties is narrowed in the two sub-regions, indicating that the intensities of the different products used vary very little at the spatial and temporal scales. RCM curves show a good agreement on the rainfall characteristic over zone 1. In contrast to zone 2, here, the RCMs simulations are more in line with Obs than the GCMs. This is confirmed by the RCMs' scores with PCC of about 0.75 in zone 1, while in zone 2, a PCC of about 0.2 is recorded. Nevertheless, in both cases, GCMs and RCMs have a variability, which is very comparable with that of Obs with SD between 1 ± 0.25 (see supplementary material; Fig. S1; pink). GCMs produce much more RR1, but less SDII than Obs in both sub-regions. This behavior could be as a result of the different dynamics used in the GCMs' parametrization. The neutralization of the contributions of these two indices in the total rainfall could explain the relative good performance of the GCMs in the seasonal cycle of the PRCPTOT over zone 1.

The seasonal cycle of CDD from Obs shows that longer dry spells occur during dry seasons (about 30 days), and shorter dry spells occur during rainy seasons (about 4 days). A better agreement between models and Obs for the seasonal cycle of CDD is particularly found in zone 1. Overall, RCM ensemble mean produces realistic simulations which are almost similar to Obs. Although a few shortcomings are still evident, in both cases, we always found that $PCC > 0.8$ and $RMSE < 1$ (see supplementary material; Fig. S1; orange).

The seasonal cycle of CWD is consistent with that of RR1 shown in Fig. 2c–d. CWD from Obs mostly range between 0 and 6 days over zone 1, whereas in zone 2, CWD does not exceed 10 days. GCMs consistently overestimate the observed CWD over both sub-regions, with curves very distant from the range of Obs uncertainties. Here, the RMSE of GCMs is always > 1.5 over both sub-regions (see supplementary material; Fig. S1; dots 1, purple). As stressed by Stephens et al. (2010), such uncertainty in GCMs could mainly be caused by radiative feedbacks from low-level clouds, which underestimate rainfall produced by these clouds, due to albedo simulation failures. However, although the length of CWD simulated by RCMs is also higher, its curve is much closer to that of Obs with $PCC > 0.85$ and $RMSE < 1$ in zone 1 (see supplementary material; Fig. S1; dot 2, purple). This result thus highlights the improvements brought about the dynamical downscaling of GCMs. Other authors have also shown that RCMs were able to better reproduce some daily rainfall indices such as dry and wet spells over CA (Dosio et al. 2015; Fotso-Nguemo et al. 2017; Vondou and Haensler 2017; Tamoffo et al. 2019).

3.1.2 Intense rainfall indices

Figure 3 presents the mean seasonal cycle of maximum 1-day rainfall amount (RX1DAY; first row), maximum consecutive 5-day rainfall amount (RX5DAY; second row), 95th percentile (R95; third row), number of wet-day rainfall above the 95th percentile (R95P; fourth row), and total wet-day rainfall amount above the 95th percentile (R95PTOT; fifth row), from Obs ensemble mean (black), GCM ensemble mean (red), and RCM ensemble mean (blue), averaged over zone 1 (first column) and zone 2 (second column), during the historical period (1998–2005). The seasonal cycle of RX1DAY exhibited by Obs is almost similar to that of RX5DAY and R95 (i.e., uni-modal and bimodal structures in zone 1 and zone 2 respectively). These indices provide an indication on the total rainfall amount which contributes to extreme weather events both in term of total amount (RX1DAY and RX5DAY)

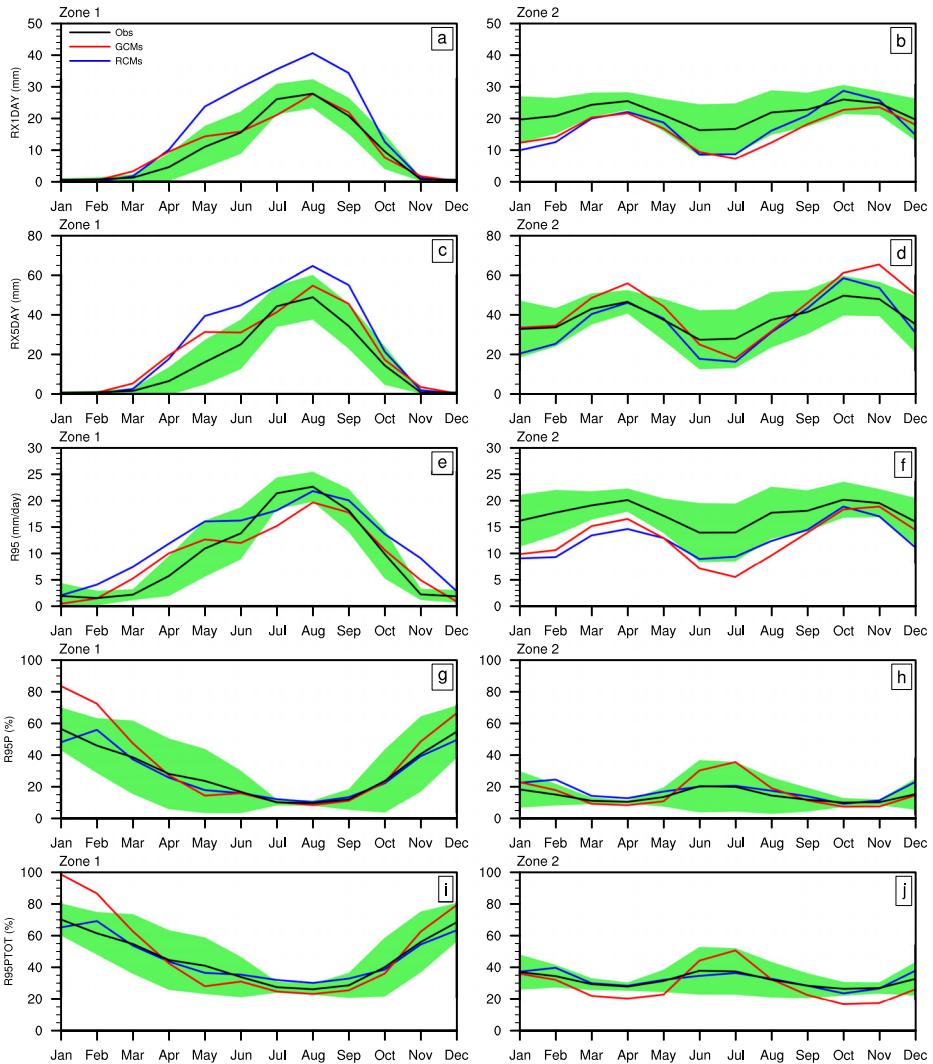


Fig. 3 Same as in Fig. 2, but for maximum 1-day rainfall amount (RX1DAY; **a, b**), for maximum consecutive 5-day rainfall amount (RX5DAY; **c, d**), 95th percentile (R95; **e, f**), number of wet-day rainfall above the 95th percentile (R95P; **g, h**), and total wet-day rainfall amount above the 95th percentile (R95PTOT; **i, j**)

and intensity (R95). Generally, both RCMs and GCMs overestimate these three indices over zone 1, while an underestimation is reported over zone 2. This suggests that the simulations fail to reproduce accurately the climatology (annual cycle) of both higher amount and intensity of rainfall events over CA. The possible cause of the overestimation of heavy rainfall amount and intensity over zone 1 could be either the horizontal resolution or the convective parametrizations, which in turn results to a poor simulation of the relationship between deep convection occurrences and heavy rainfall (Crétat et al. 2015).

Over both sub-regions, the seasonal cycle of R95P indicates that there are generally good agreements between Obs and RCMs, with lower number of occurrence (about 20 %) found

during rainy seasons. This implied that during the rainy season most of the rainfall is not associated with the occurrence of very wet-day events. RCMs appear to generally improve GCMs that largely overestimate the frequency of heavy rainfall events compared with the Obs, especially during pre- and post-monsoon months. This improvement is mainly due to the variability of the RCMs which is clearly better than that of the GCMs over the two sub-regions (see supplementary material; Fig. S1; red). Such improvement could result from cancellation of errors among the different RCMs members.

The seasonal cycle of R95PTOT is generally similar to that of R95P showing minimum values which coincides with the rainy seasons' peaks over the studied sub-regions. During rainy seasons, a contribution of about 30 % to the total rainfall amount is reported in Obs, indicating that extreme rainfall events greater than the 95th percentile are not the most important contributor to the total rainfall amount. RCMs are generally able to successfully capture the seasonal cycle of R95PTOT, especially in zone 2 where the RCMs show a PCC exceeding 0.75, along with a variability almost equal to that of Obs (see supplementary material; Fig. S1; blue). Overall, despite the magnitude of R95PTOT is slightly overestimated compared with Obs during June–October over zone 1, RCMs clearly improve the GCM results.

Overall, this analysis shows that RCM ensemble mean captures quite well the observed seasonal cycle of extreme rainfall events over CA with few discrepancies. This good performance of the RCM ensemble mean is particularly observed over zone 2 where it is able to reduce or cancel the strong GCM ensemble mean's bias throughout the seasonal cycle of rainfall events.

3.2 Climate change of extreme rainfall indices

3.2.1 Change in duration and intensity-based indices

Figure 4 displays the multi-model ensemble mean change (in %) for PRCPTOT (first row), RR1 (second row), SDII (third row), CWD, and CDD (fifth row), during the middle ($p1 = 2029–2058$, blue) and late twenty-first century ($p2 = 2069–2098$, red), relative to the baseline historical time period (1976–2005). The RCM ensemble means change in the seasonal cycle of PRCPTOT for the two sub-regions showing a decrease (up to 15 % at June over zone 1) which is generally not significant. A slight increase in PRCPTOT is observed just after the rainy season (September–October), particularly over north-eastern Democratic Republic of Congo (see supplementary material; Fig. S2b, first row). Changes in PRCPTOT are suggestive of a general reduction of rainfall throughout the year and especially during pre-monsoon months, but are more marked at the late twenty-first century.

Changes in seasonal cycle of RR1 from RCMs also show a significant decrease throughout the year followed by a slight increase during October–December over zone 1. Note that their curves are consistent with that of PRCPTOT (i.e., projected a decrease throughout the year), with peaks during pre-monsoon months. Highest decrease ($>20\%$) is found over zone 1, with largest and more significant areas during late twenty-first century (see supplementary material; Fig. S2a–b; second row). On the other hand, RCMs' changes in seasonal cycle of SDII show a significant increase of about 20 % over zone 1 and 14 % over zone 2, which remains almost unchanged during the year. Recently, similar results showing increasing wet-day intensity have been reported over CA (Sonkoué et al. 2018). For SDII curves, timing of the maximum values seems to coincide with that of monsoon seasons over the two sub-regions shown in Fig. 2a–b. Therefore, the decrease found in total wet-day rainfall amount is associated only with change of wet-day frequency and not with the combination

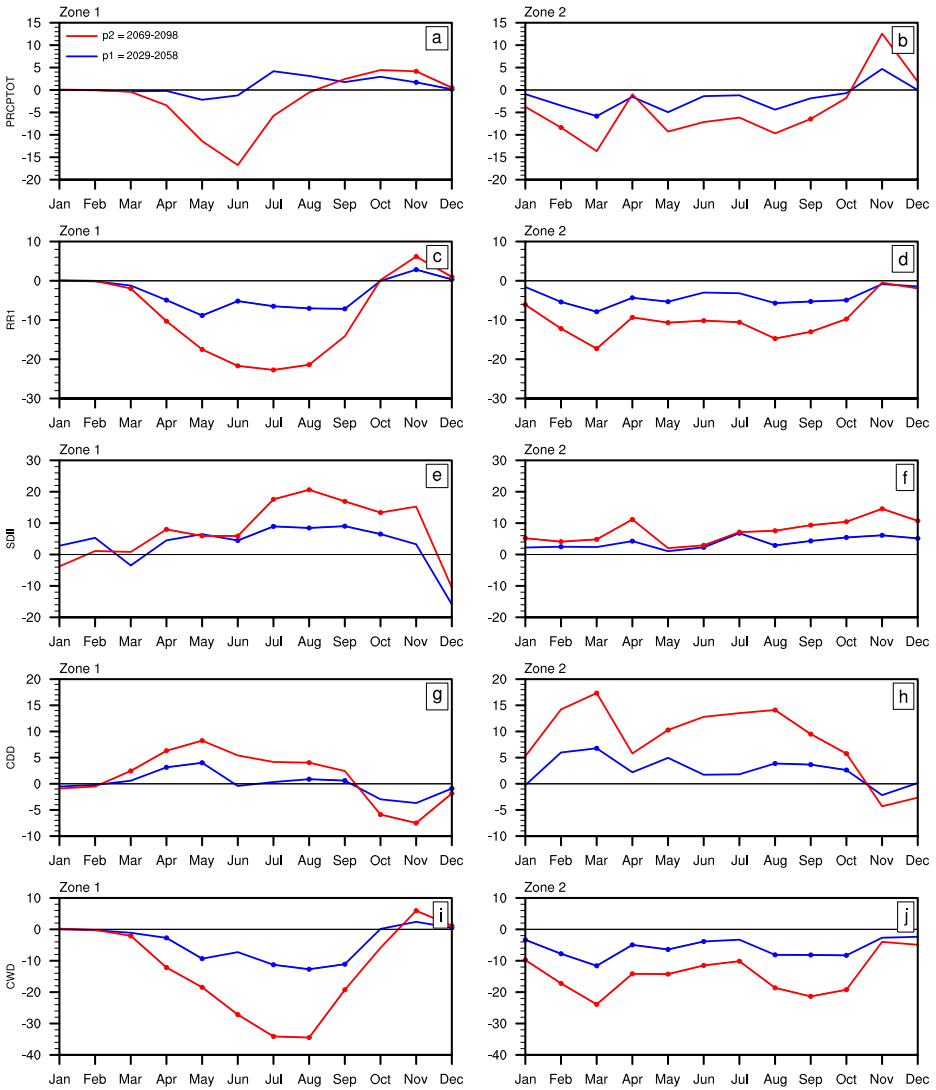


Fig. 4 Projected change (in %) in the seasonal cycle for total wet-day rainfall amount (PRCPTOT; **a, b**), wet-day frequency (RRI; **c, d**), wet-day intensity (SDII; **e, f**), dry spell (CDD; **g, h**) and wet spell (CWD; **i, j**), over zone 1 (first column) and zone 2 (second column), from RCMs ensemble mean during the middle ($p1 = 2029–2058$, blue) and late twenty-first century ($p2 = 2069–2098$, red), relative to the baseline historical time period (1976–2005). Dots on lines indicate months where the change is significant (i.e., where at least 80 % of simulations agree on the sign of the change)

of both wet-day frequency and intensity as documented in Sylla et al. (2015) over the West African region.

Concerning changes in CDD, its seasonal cycle shows a significant increase during pre-monsoon months over both sub-regions, followed by a decrease at the end of year. Over zone 1, the decrease in CDD recorded between September and December seems to be influenced by the increase in RRI during the same period. Note that area extended where CDD

increases coincides with those where RR1 decreases (see supplementary material; Fig. S2a–b; second and fourth rows). Contrariwise, changes in the seasonal cycle of CWD show a significant decrease over both sub-regions throughout the year with decreasing peaks which almost coincide with those of PRCPTOT and RR1. In general, CDD (CWD) is projected to increase (decrease) over the entire CA with shorter (longer) dry (wet) spells projected during pre-monsoon months. However, the area of increase (decrease) of CDD (CWD) is more pronounced during late twenty-first century (see supplementary material; Fig. S2a–b, fourth and fifth rows). Increases in dry spells coupled with decrease in wet spells and wet-day frequency could have strong consequences for seasonal rainfall onset, along with total yearly rainfall amount over CA. This implied that countries within these two sub-regions of CA could experience a more extended dry season; therefore, would be exposed to high drought risk in the future. Such changes induced by the global warming could likely threaten water resources availability, which can impact the rain-fed agriculture, hydroelectric power generation, and water resources management.

3.2.2 Change in intense rainfall indices

Figure 5 presents the multi-model ensemble mean change (in %) for RX1DAY (first row), RX5DAY (second row), R95 (third row), R95P (fourth row), and R95PTOT (fifth row), during the middle ($p1 = 2029–2058$, blue) and late twenty-first century ($p2 = 2069–2098$, red), relative to the baseline historical time period (1976–2005). The projected changes in the seasonal cycle of RX1DAY exhibited by RCMs are almost similar to those of RX5DAY and R95. The temporal pattern of these three indices shows a significant increase of about 10–45 % throughout the year, with higher values in the case of RX1DAY. The timing of their maximum values coincides with rainy season's peak over these two sub-regions, except for the second rainy season (September–November) in zone 2 where a delay (lag) of 1 month is reported. Pattern of increase areas is more significant and more extended during the late twenty-first century for RX1DAY than for RX5DAY and R95 (see supplementary material; Fig. S3a–b, first to third rows). This result is consistent with the increase in RX5DAY found by Pokam et al. (2018) over CA with an ensemble mean of twenty-five (25) RCMs.

The projected seasonal cycle of R95P exhibited by RCMs shows a significant negative change of about 4–8 %, which follows the change of PRCPTOT and RR1 over both sub-regions. Peaks of this change appear only during pre-monsoon months (i.e., April for zone 1; February and July for zone 2). In addition, these peaks occur 1–2 months before those of PRCPTOT and RR1 shown in Fig. 4a–d over the two sub-regions. This result suggests that during the pre-monsoon period, the decrease in occurrence of heavy rainfall could be a precursor to the decrease of wet-day frequency and thus of total wet-day rainfall amount. This behavior can worsen water stress over north-eastern Nigeria, northern Cameroon, southern Chad, and northern Zambia (see supplementary material; Fig. S3a–b, fourth row); since the occurrence of its minimum during the historical period has a contribution of about 40 % to the frequency of heavy rainfall events. Nevertheless, although it is not significant, the increase in R95P observed during post-monsoon months could explain the increase in PRCPTOT and RR1 found over zone 1.

Changes in seasonal cycle of R95PTOT as simulated by RCMs show a significant increase (up to 35 %) from July to December over both sub-regions for both periods, but are more accentuated during the late twenty-first century. The timing of increase R95PTOT's peaks corresponds with that of rainy season's peak over the two sub-regions. Generally, the spatial and temporal increase patterns of R95PTOT follow the change in SDII, RX1DAY, RX5DAY, and R95, indicating that these later share common features. This means that

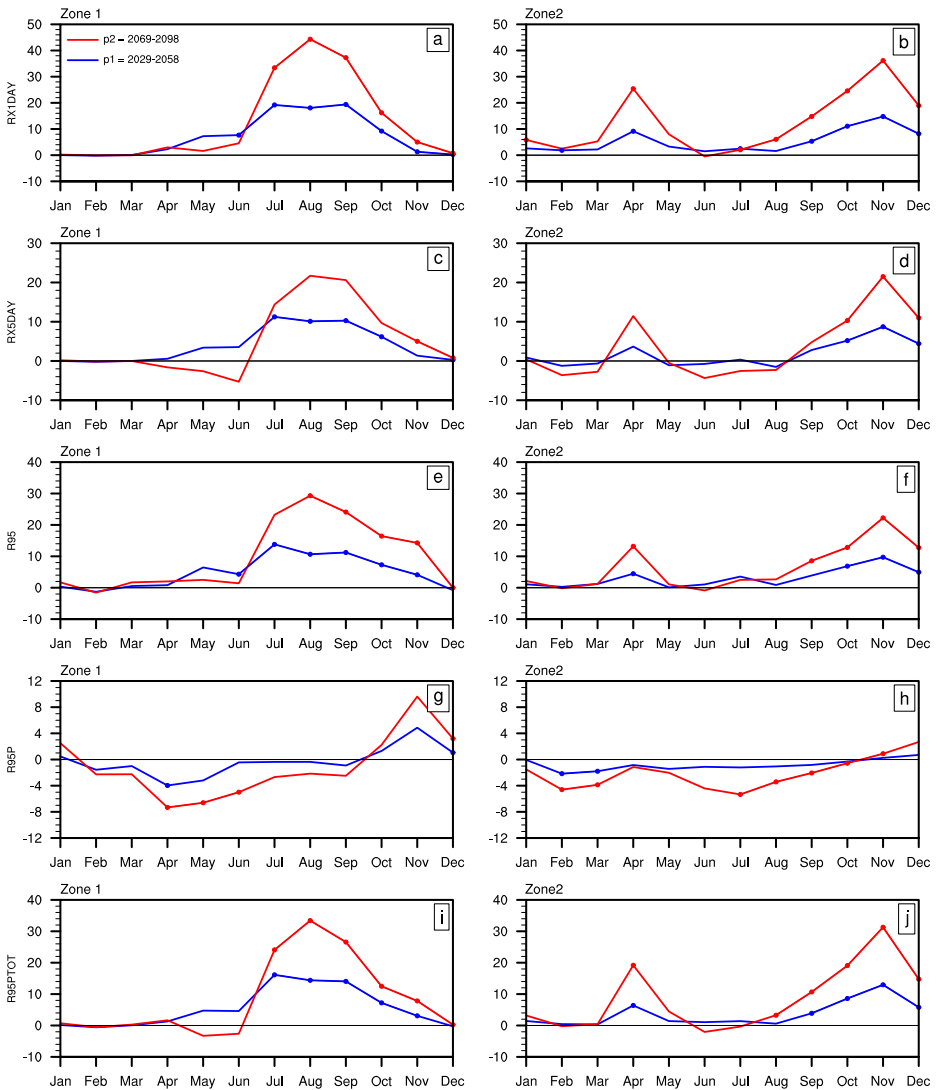


Fig. 5 Same as in Fig. 5, but for maximum 1-day rainfall amount (RX1DAY; **a, b**), maximum consecutive 5-day rainfall amount (RX5DAY; **c, d**), 95th percentile (R95; **e, f**), number of wet-day rainfall above the 95th percentile (R95P; **g, h**), and total wet-day rainfall amount above the 95th percentile (R95PTOT; **i, j**)

extreme rainfall events could be more intense both in terms of rainfall amount (RX1DAY, RX5DAY, and R95PTOT) and intensity (SDII and R95), which is likely to enhance the probability of flood risks during monsoon months. This result is particularly important as these recent years, countries crossed by CA have experienced an increase in flood phenomena during rainy seasons. For example, the most recent events are 3rd of March 2016 in Kinshasa (Democratic Republic of Congo), 18th of February 2017 in Libreville (Gabon), 3rd of July 2017 in Douala (Cameroon), and 24th of August 2017 in Bangui (Central African Republic), causing huge financial losses and many victims. The increase of intense rainfall

events found here is in line with other previous studies carried out over Africa, based on GCMs and/or RCMs (e.g., Haensler et al. 2013; Sylla et al. 2015; Diallo et al. 2016; Fotso-Nguemo et al. 2018; Pokam et al. 2018; Sonkoué et al. 2018). In their studies, they have shown that the spatial distribution of intense rainfall events could significantly increase over their respective study areas, especially during the monsoon periods.

The dynamical mechanisms linked to the reported changes generally vary according to regions, time scales, and the type of model used for the analysis. However, some important factors such as (i) large-scale natural variability through atmospheric variables (temperature, rainfall, cloud cover, or the occurrence of storms; (ii) anthropogenic GHG concentration changes; and (iii) land use/land cover change play a key role (IPCC 2013). For instance, our results show that while the amount and intensity of heavy rainfall events greatly increase during rainy seasons (10–45 %), especially over zone 1, the frequency of occurrence of these events slightly decreases (4–8 %). This implies that heavy rainfall events are likely to increase during monsoon months. We can thus conclude that under global warming, CA rainfall shifts toward a regime of more intense and less frequent extreme rainfall events. Dyer et al. (2017) attributed this extreme rainfall response to an increase of moisture convergence intensified by the presence of the Congo Basin rainforest. This interpretation was consistent to the results of Sylla et al. (2015), done over West Africa, who associated increases of intense rainfall events to increase of moisture convergence in the boundary layer, driven by larger amounts of moist static energy and instability. On the other hand, the analysis of total rainfall amount and duration-based indices (frequency, dry and wet spells) also reveal that certain locations of CA could experience high drought risk in the future. This will be mainly tied to the combined decrease of total rainfall amount and their number of occurrence. One possible explanation of this trend to the dryness of CA is associated with the anomalously sea surface temperature cooling over the Atlantic and/or Indian Ocean, which reduces the release of latent heat flux and weakens the Walker circulation (Cook and Vizi 2015; Hua et al. 2016).

4 Summary and conclusions

In this study, the projected seasonal cycle of ten extreme rainfall indices was investigated over CA in order to understand the vulnerability of the region to climate change. An ensemble mean of seven gridded Obs and six RCM experiments, driven by seven GCMs (a total of fifteen members), have been analysed. We firstly evaluate their performance, and secondly describe the characteristics of daily rainfall indices as simulated by RCMs for the middle and late twenty-first century, under the high GHG scenario (RCP8.5). Results of our analysis are summarised as follows:

- Although some differences still exist between Obs and models, RCMs were able to reproduce reliably the climatology of daily rainfall indices over the analysed sub-regions, with biases which are within the Obs uncertainties in most cases.
- Contrary to the results found over West Africa (Sylla et al. 2015; Diallo et al. 2016), in addition to wet-day frequency, wet-day intensity also contributes to the bimodal structure of the seasonal cycle of rainfall in zone 2, dominated by a tropical rainforest climate.
- For both the middle and the late twenty-first century, a general non-significant decrease in total wet-day rainfall amount is projected over the two analysed sub-regions, especially during pre-monsoon months.

- A prevailing significant decrease in wet-day frequency is projected over whole CA, while wet-day intensity is projected to significantly increase. This implies that the increase in wet-day intensity is not responsible for the decrease in total wet-day rainfall amount over these sub-regions.
- Dry (wet) spells are projected to significantly increase (decrease) over both sub-regions with shorter (longer) dry (wet) spells projected during pre-monsoon months. This suggests that countries within these two sub-regions could likely experience high drought risk in the future, mainly caused by the combined effect of decrease of total rainfall amount and their number of occurrence.
- The projected changes in maximum daily rainfall amount, maximum 5-day rainfall amount, and 95th percentile show a significant increase of about 10–45 % during monsoon months, with higher values in the case of maximum daily rainfall amount.
- The total number of occurrence of rainfall events above the 95th percentile project a slight significant decrease of about 4–8 % during pre-monsoon month, while the total amount of rainfall events above the 95th percentile project a significant increases of about 10–45 % during monsoon months. This implies that heavy rainfall events are likely to be more intense, and could amplify the probability of flood risks during monsoon months over both sub-regions, especially in August for zone 1, April and November for zone 2.

Thereby, the increase (decrease) in extreme rainfall events (total rainfall amount), which occurred during monsoon phases (pre-monsoon phases), could have a direct impact on water resources availability in the region. Effective adaptation and mitigation measures are thus required to help design strong subregional policies, and therefore prevent the potential impact of climate change on future rainfall extremes events.

Acknowledgments The first author gratefully acknowledge all researcher of LPAO-SF for their close collaboration during his stay at Dakar. This work is part of the LMI DYCOFAC initiative for which we would like to express our gratitude. We would like to thank the GERICS for providing the REMO datasets through the project “*Climate Change Scenarios for the Congo Basin*”. We are also grateful to all other modelling groups that performed CORDEX and CMIP5 simulations used in this study, which are freely available through the website “<https://climate4impact.eu/impactportal/data/esgfsearch.jsp>”. Many thanks also go to the two anonymous reviewers along with the editor for their constructive suggestions, which have greatly improved the quality of the paper.

Funding information This work was supported by the inter-university/intra-ACP mobility program PAFROID, which has been funded with the support of the European Commission (reference 384201-EM-1-2013-1-MG-INTRA-ACP).

References

- Almer C, Laurent-Lucchetti J, Oechslin M (2017) Water scarcity and rioting: disaggregated evidence from Sub-Saharan Africa. *J Environ Econ Manag* 86:193–209. <https://doi.org/10.1016/j.jeem.2017.06.002>
- Ashouri H, Hsu KL, Sorooshian S, Braithwaite DK, Knapp KR, Cecil LD, Nelson BR, Prat OP (2015) PERSIANN-CDR: daily precipitation climate data record from multisatellite observations for hydrological and climate studies. *Bull Am Meteorol Soc* 96:69–83
- Beck HE, Van Dijk AI, Levizzani V, Schellekens J, Gonzalez Miralles D, Martens B, De Roo A (2017) MSWEP: 3-hourly 0.25 global gridded precipitation (1979–2015) by merging gauge, satellite, and reanalysis data. *Hydrol Earth Syst Sci* 21:589–615
- Cook KH, Vizy E (2015) The Congo basin walker circulation: dynamics and connections to precipitation. *Clim Dyn*. <https://doi.org/10.1007/s00382-015-2864-y>





- Crétat J, Vizy EK, Cook KH (2015) The relationship between African easterly waves and daily rainfall over West Africa: observations and regional climate simulations. *Clim Dyn* 44:385–404. <https://doi.org/10.1007/s00382-014-2120-x>
- Diallo I, Sylla MB, Giorgi F, Gaye AT, Camara M (2012) Multimodel GCM-RCM ensemble-based projections of temperature and precipitation over West Africa for the early 21st century. *Int J Geophys* 2012:1–19. <https://doi.org/10.1155/2012/972896>
- Diallo I, Bain CL, Gaye AT, Moufouma-Okia W, Niang C, Dieng MDB, Graham R (2014) Simulation of the West African monsoon onset using the HadGEM3-RA regional climate model. *Clim Dyn* 43:575–594. <https://doi.org/10.1007/s00382-014-2219-0>
- Diallo I, Giorgi F, Deme A, Tall M, Mariotti L, Gaye AT (2016) Projected changes of summer monsoon extremes and hydroclimatic regimes over West Africa for the twenty-first century. *Clim Dyn* 47:3931–3954. <https://doi.org/10.1007/s00382-016-3052-4>
- Dommo A, Philippon N, Vondou DA, Sèze G, Eastman R (2018) The June–September low cloud cover in Western Central Africa: mean spatial distribution and diurnal evolution, and associated atmospheric dynamics. *J Clim* 31:9585–9603. <https://doi.org/10.1175/JCLI-D-17-0082.1>
- Dosio A, Panitz HJ, Schubert-Frisius M, Lüthi D (2015) Dynamical downscaling of CMIP5 global circulation models over CORDEX-Africa with COSMO-CLM: evaluation over the present climate and analysis of the added value. *Climate Dynam* 44:2637–2661
- Dyer ELE, Jones DBA, Nusbaumer J, Li H, Collins O, Vettoretti G, Noone D (2017) Congo Basin precipitation: assessing seasonality, regional interactions, and sources of moisture. *J Geophys Res Atmos* 122:6882–6898. <https://doi.org/10.1002/2016JD026240>
- Fotso-Nguemo TC, Vondou DA, Tchawoua C, Haensler A (2016) Assessment of simulated rainfall and temperature from the regional climate model REMO and future changes over Central Africa. *Clim Dyn* 48:3685–3705. <https://doi.org/10.1007/s00382-016-3294-1>
- Fotso-Nguemo TC, Vondou DA, Pokam WM, Djomou ZY, Diallo I, Haensler A, Tchotchou LAD, Kamsu-Tamo PH, Gaye AT, Tchawoua C (2017) On the added value of the regional climate model REMO in the assessment of climate change signal over Central Africa. *Clim Dyn* 49:3813–3838. <https://doi.org/10.1007/s00382-017-3547-7>
- Fotso-Nguemo TC, Chamani R, Yepdo ZD, Sonkoué D, Matsaguim CN, Vondou DA, Tanessong RS (2018) Projected trends of extreme rainfall events from CMIP5 models over Central Africa. *Atmos Sci Lett* 19:1–8. <https://doi.org/10.1002/asl.803>
- Funk C, Peterson P, Landsfeld M, Pedreros D, Verdin J, Rowland J, Romero B, Husak G, Michaelsen J, Verdin A (2014) A quasi-global precipitation time series for drought monitoring: U.S. geological survey data series 832. *Wiley Interdiscip Rev: Climate Change* 2:4. <https://doi.org/10.3133/ds832>
- Giorgi F, Jones C, Asrar GR (2009) Addressing climate information needs at the regional level: the CORDEX framework. *WMO Bull* 58:175–183
- Haensler A, Saeed F, Jacob D (2013) Assessing the robustness of projected precipitation changes over central Africa on the basis of a multitude of global and regional climate projections. *Clim Change* 121:349–363. <https://doi.org/10.1007/s10584-013-0863-8>
- Hua W, Zhou L, Chen H, Nicholson SE, Raghavendra A, Jiang Y (2016) Possible causes of the Central Equatorial African long-term drought. *Environ Res Lett* 11:124,002. <https://doi.org/10.1088/1748-9326/11/12/124002>
- Huffman GJ, Bolvin DT, Nelkin EJ, Wolff DB, Adler RF, Gu G, Hong Y, Bowman KP, Stocker EF (2007) The TRMM multi-satellite precipitation analysis: quasi-global, multi-year, combined-sensor precipitation estimates at fine scale. *J Hydrometeorol* 8:33–55
- Huffman GJ, Adler RF, David TB, Guojun G (2009) Improving the global precipitation record: GPCP Version 2.1. *Geophys Res Lett* 36:1–5. <https://doi.org/10.1029/2009GL040000>
- IPCC (2013) Summary for Policymakers. In: *Climate change 2013: the physical science basis contribution of working group I to the fifth assessment report of the intergovernmental panel on climate change*. Cambridge University Press, Cambridge
- Jacquet J, Jamieson D (2016) Soft but significant power in the Paris agreement. *Nat Clim Change* 6:643–646
- Joyce RJ, Janowiak JE, Arkin PA, Xie P (2004) CMORPH: a method that produces global precipitation estimates from passive microwave and infrared data at high spatial and temporal resolution. *J Hydrometeorol* 5:487–503
- Kamsu-Tamo PH, Janico S, Monkam D, Lenou A (2014) Convection activity over the Guinean coast and Central Africa during northern spring from synoptic to intra-seasonal timescales. *Clim Dyn* 43:3377–3401. <https://doi.org/10.1007/s00382-014-2111-y>
- Klutse NAB, Sylla MB, Diallo I, Sarr A, Dosio A, Diedhiou A, Kamga A, Lamptey B, Ali A, Gbobaniyi EO, Owusu K, Lennard C, Hewitson B, Nikulin G, Panitz HJ, Büchner M (2016) Daily characteristics of West

- African summer monsoon precipitation in CORDEX simulations. *Theor Appl Climatol* 123:369–386. <https://doi.org/10.1007/s00704-014-1352-3>
- Mariotti L, Diallo I, Coppola E, Giorgi F (2014) Seasonal and intraseasonal changes of African monsoon climates in 21st century CORDEX projections. *Clim Change* 125:53–65. <https://doi.org/10.1007/s10584-014-1097-0>
- Moss RH, Edmonds J, Hibbard K, Manning MR, Rose SK, van Vuuren DP, Carter TR, Emori S, Kainuma M, Kram T, Meehl G, Mitchell JFB, Nakicenovic N, Riahi K, Smith SJ, Stouffer RJ, Thomson AM, Weyant JP, Wilbanks TJ (2010) The next generation of scenarios for climate change research and assessment. *Nature* 463:747–756. <https://doi.org/10.1038/nature08823>
- Nikulin G, Jones C, Samuelsson P, Giorgi F, Asrar G, Büchner M, Cerezo-Mota R, Christensen OB, Déqué M, Fernandez J, Hänsler A, van Meijgaard E, Sylla MB, Sushama L (2012) Precipitation climatology in an ensemble of CORDEX-Africa regional climate simulations. *J Climate* 25:6057–6078. <https://doi.org/10.1175/JCLI-D-11-00375.1>
- Novella NS, Thiaw WM (2013) African rainfall climatology version 2 for famine early warning systems. *J Appl Meteorol Climatol* 52:588–606
- Pinto I, Lennard C, Tadross M, Hewitson B, Dosio A, Nikulin G, Panitz HJ, Shongwe ME (2016) Evaluation and projections of extreme precipitation over southern Africa from two CORDEX models. *Clim Change* 135:655–668. <https://doi.org/10.1007/s10584-015-1573-1>
- Pokam MW, Bain CL, Chadwick RS, Graham R, Sonwa DJ, Kamba FM (2014) Identification of processes driving low-level westerlies in West Equatorial Africa. *J Climate* 27:4245–4262. <https://doi.org/10.1175/JCLI-D-13-00490.1>
- Pokam MW, Longandjo GN, Moufouma-Okia W, Bell JP, James R, Vondou DA, Haensler A, Fotso-Nguemo TC, Guenang GM, Tchotchou ALD, Kamsu-Tamo PH, Takong RR, Nikulin G, Lennard CJ, Dosio A (2018) Consequences of 1.5 °C and 2 °C global warming levels for temperature and precipitation changes over Central Africa. *Environ Res Lett* 13:1–12. <https://doi.org/10.1088/1748-9326/aab048>
- Saha F (2015) Les changements climatiques et la vulnérabilité des villes d'Afrique centrale aux risques naturels : cas des inondations et des mouvements de masse à Bamenda (nord-ouest du Cameroun). *Edilivre-Aparis, Classique*, p 206
- Seneviratne S, Nicholls N, Easterling D, Goodess C, Kanae S, Kossin J, Luo Y, Marengo J, McInnes K, Rahimi M, Reichstein M, Sorteberg A, Vera C, Zhang X (2012) Changes in climate extremes and their impacts on the natural physical environment. In: Field CB, Barros V, Stocker TF, Qin D, Dokken DJ, Ebi KL, Mastrandrea MD, Mach KJ, Plattner G-K, Allen SK, Tignor M, Midgley PM (eds) A special report of working groups I and II of the intergovernmental panel on climate change (IPCC). Cambridge University Press, Cambridge, pp 109–230
- Sonkoué D, Monkam D, Fotso-Nguemo TC, Yepdo DZ, Vondou DA (2018) Evaluation and projected changes in daily rainfall characteristics over Central Africa based on a multi-model ensemble mean of CMIP5 simulations. *Theor Appl Climatol*, 1–20. <https://doi.org/10.1007/s00704-018-2729-5>
- Sonwa DJ, Somorin OA, Jum C, Bele MY, Nkem JN (2012) Vulnerability, forest-related sectors and climate change adaptation: the case of Cameroon. *For Policy Econ* 23:1–9
- Stephens GL, L'Ecuyer T, Forbes R, Gettleman A, Golaz J, Bodas-Salcedo A, Suzuki K, Gabriel P, Haynes J (2010) Dreary state of precipitation in global models. *J Geophys Res-Atmos* 115:D24,211. <https://doi.org/10.1029/2010jd014532>
- Sylla MB, Giorgi F, Coppola E, Mariotti L (2013) Uncertainties in daily rainfall over Africa: assessment of observation products and evaluation of a regional climate model simulation. *Int J Climatol* 33:1805–1817. <https://doi.org/10.1002/joc.3551>
- Sylla MB, Giorgi F, Pal JS, Gibba P, Kebe I, Nikiema M (2015) Projected changes in the annual cycle of high-intensity precipitation events over West Africa for the late twenty-first century. *J Climate* 28:6475–6488. <https://doi.org/10.1175/JCLI-D-14-00854.1>
- Tamoffo AT, Vondou DA, Pokam WM, Haensler A, Yepdo DZ, Fotso-Nguemo TC, Tchotchou LAD, Nouayou R (2019) Daily characteristics of Central African rainfall in the REMO model. *Theor Appl Climatol*, 1–18. <https://doi.org/10.1007/s00704-018-2745-5>
- Tanessong RS, Vondou DA, Djomou ZY, Igrí PM (2017) WRF high resolution simulation of an extreme rainfall event over Douala (Cameroon): a case study. *Model Earth Syst Environ* 3:927–942. <https://doi.org/10.1007/s40808-017-0343-7>
- Taylor KE (2001) Summarizing multiple aspects of model performance in a single diagram. *J Geophys Res* 106:7183–7192
- Taylor KE, Stouffer RJ, Meehl GA (2012) An overview of CMIP5 and the experiment design. *Bull Am Meteorol Soc* 93:485–498. <https://doi.org/10.1175/BAMS-D-11-00094.1>

- Vondou DA, Haensler A (2017) Evaluation of simulations with the regional climate model REMO over Central Africa and the effect of increased spatial resolution. *Int J Climatol* 37:741–760. <https://doi.org/10.1002/joc.5035>
- Vondou DA, Nzeukou A, Kanga FM (2010) Diurnal cycle of convective activity over the West of Central Africa based on meteosat images. *Int J Appl Earth Observ Geoinf* 12:58–62
- Zebaze S, Lenouo A, Tchawoua C, Gaye AT, Kanga FM (2017) Interaction between moisture transport and Kelvin waves events over Equatorial Africa through ERA-interim. *Atmos Sci Let* 18:300–306. <https://doi.org/10.1002/asl.756>
- Zhang X, Alexander L, Hegerl GC, Jones P, Tank AK, Peterson TC, Trewin B, Zwiers FW (2011) Indices for monitoring changes in extremes based on daily temperature and precipitation data. *Wiley Interdiscip Rev: Climate Change* 2:851–870. <https://doi.org/10.1002/wcc.147>

Publisher's note Springer Nature remains neutral with regard to jurisdictional claims in published maps and institutional affiliations.

Affiliations

Thierry C. Fotso-Nguemo^{1,2}  · Ismaïla Diallo³  · Moussa Diakhaté⁴  ·
Derbetini A. Vondou^{2,5}  · Mamadou L. Mbaye⁶ · Andreas Haensler⁷ ·
Amadou T. Gaye⁴ · Clément Tchawoua⁸

¹ Climate Change Research Laboratory (CCRL), National Institute of Cartography, P.O. Box 157 Yaounde, Cameroon

² Laboratory for Environmental Modelling and Atmospheric Physics (LEMAP), Department of Physics, Faculty of Science, University of Yaounde 1, P.O. Box 812 Yaounde, Cameroon

³ Department of Geography, University of California Los Angeles (UCLA), Los Angeles, CA 90095, USA

⁴ Laboratoire de Physique de l'Atmosphère et de l'Océan Siméon Fongang (LPAO-SF), Ecole Supérieure Polytechnique, Université Cheikh Anta Diop, P.O. Box 5085 Dakar, Sénégal

⁵ Laboratoire Mixte International “Dynamique des écosystèmes continentaux d’Afrique Centrale en contexte de changements globaux” (LMI DYCOFAC), Institut de Recherche pour le Développement, P.O. Box 1857 Yaounde, Cameroon

⁶ Département de Physique, Unité de Formation et de Recherches en Sciences et Technologies (UFR-ST), Université Assane Seck, P.O. Box 523 Ziguinchor, Sénégal

⁷ Climate Service Center Germany (GERICS), Helmholtz-Zentrum Geesthacht, Fischertwierte 1, Hamburg, Germany

⁸ Laboratory of Mechanics, Department of Physics, Faculty of Science, University of Yaounde 1, P.O. Box 812 Yaounde, Cameroon